Advances in Water Resources 34 (2011) 1553–1562

Contents lists available at SciVerse ScienceDirect

Advances in Water Resources

journal homepage: www.elsevier.com/locate/advwatres

Transient analysis for fluid injection into a dome reservoir

Chia-Chen Kuo [a,b], Ching-Sheng Huang [a], Hund-Der Yeh [a,*]

[a] Institute of Environmental Engineering, National Chiao Tung University, Hsinchu 300, Taiwan
[b] National Center for High-performance Computing, National Applied Research Laboratories, Hsinchu 300, Taiwan

ARTICLE INFO

Article history:
Received 24 January 2011
Received in revised form 5 July 2011
Accepted 18 August 2011
Available online 10 September 2011

Keywords:
Analytical solution
Bromwich integral method
Dome reservoir
Laplace transform
Sensitivity analysis
Well injection

ABSTRACT

A dome-shaped layer can be selected as a storage site for fluid injection. In this study, we develop a mathematical model for simulating transient head distribution in a heterogeneous and anisotropic dome-shaped layer due to a constant-head injection in a fully penetrating well. In the model, a form of step change is adopted to approximate the upper and lower boundaries of the dome and then the layer is split into two regions. The Laplace-domain solution of the model is developed using the Laplace transform and method of separation of variables. The transient injection rate at wellbore can then be obtained based on Darcy's law and Bromwich integral method. The predicted head contours from the head solution show significant vertical flow components near the location of step change in the dome reservoir. The results of sensitivity analysis indicate that the hydraulic conductivity is the most sensitive parameter and the specific storage is the least sensitive one to the injection rate after a short period of injection time. In addition, the injection rate for a dome reservoir is also very sensitive to the change of the height for the reservoir near the injection well (first region) at a very early injection time. In contrast, the injection rate is more sensitive to the change of the height of the second region than that of the first region at late time. This analytical solution may be used as a primary tool to assess the capacity of fluid injection to various dome reservoirs.

1. Introduction

A salt dome, known as a diapir, with a dual convex-upward structure is usually produced by vertical crustal movements of gravitational forces acting on a salt bed which has a lower density than surrounding material [1]. Since a salt dome gives a physical trapping mechanism [2], it may naturally be considered as an oil reservoir [3,4] or selected as a storage site for injection of liquid waste or carbon dioxide (CO_2) [2,4]. Accordingly, there is a need to develop a tool to assess the storage capacity or analyze the flow field due to underground injection.

Some mathematical models had been developed for describing the behavior of flow field due to pumping or injecting in horizontal aquifers. Nordbotten et al. [5] developed analytical solutions to estimate leakage from abandoned wells near injecting wells in multiple-layer aquifers during the process of waste injection. Kirkham [6] derived an analytical solution for investigating steady-state head distribution for a constant-head injection in a confined aquifer with a finite-radius and partially penetrating well. Using a similar solution procedure proposed by Kirkham [6], Javandel and Zaghi [7] developed an analytical solution to describe steady-state head distribution due to constant-head extraction from an extended well which has a finite thickness disk at the bottom of the aquifer.

Most of domes are formed with bent shape due to regional compression. Al-Mohannadi et al. [8] used a finite-difference model to analyze the behavior of the flow field induced from an injecting well in a single-layer dome. They found that the curve boundary of anticline has significant effects on fluid injection. Yeh and Kuo [9] used a step change approach to approximate the upper curve boundary of a single-layer anticline in which the lower boundary is flat. Based on this approximation, they developed an analytical solution for describing steady-state head distribution induced from injection or extraction in a fully penetrating well.

The objective of this paper is to develop a mathematical model for simulating transient flow in a dome reservoir fully penetrated by an injecting well under constant head condition. The step change approach is employed to approximate the upper and lower curved boundaries of the dome reservoir. The domain in radial direction is then divided into two regions where the first region starts from the rim of well radius and the other extends infinitely from the interface between these two regions. The Laplace-domain solution of the model is first developed for describing the transient head distribution in the dome reservoir. Then, the time domain results for the head distribution are evaluated using the Stehfest algorithm [10]. Furthermore, the solution in time domain for describing transient injection rate at the wellbore can be acquired

* Corresponding author. Tel.: +886 3 5731910; fax: +886 3 5725958.
E-mail address: hdyeh@mail.nctu.edu.tw (H.-D. Yeh).

0309-1708/$ - see front matter © 2011 Elsevier Ltd. All rights reserved.
doi:10.1016/j.advwatres.2011.08.006

Nomenclature

a_0	constant used in (13) and (14)
a_m	constants used in (13)
b_n	constants used in (14)
$\tilde{c}_1$, $\tilde{c}_2$, $\tilde{c}_3$	constants defined by (B4)
m, n	positive integers
p	Laplace variable
r	radial coordinate
r_1	distance from the center of the injection well to the interface between regions 1 and 2 (trap width)
r_2	well radius
r'	radius from the origin defined in complex plane
h_i	heads used in (1)
h_1	head for region 1
h_2	head for region 2
s_w	head at the wellbore
$\bar{h}_i$	heads used in (A1)
$\bar{h}_1$	head used in (13)
$\bar{h}_2$	head used in (14)
t	time
u	dummy variable
z	vertical coordinate
z_0	$z_1 + \Delta_1$ or $z_2 + \Delta_2$
z_1	aquifer thickness of region 1
z_2	aquifer thickness of region 2
z_e	$z_1 - \Delta_2$ or $z_2 - \Delta_1$
I_0	modified Bessel function of the first kind of order zero
I_1	modified Bessel function of the first kind of order one
J_0	modified Bessel function of the first kind of order zero
J_1	modified Bessel function of the first kind of order one
K_0	modified Bessel function of the second kind of order zero
K_1	modified Bessel function of the second kind of order one
P_i	the ith parameter used in (25) and (26)
$Q_w(p)$	volumetric flow rate in Laplace domain defined by (C3)
$Q_w(t)$	volumetric flow rate in time domain defined by (20)
$S_{i,t}$	normalized sensitivity at time t for the ith parameter defined by (26)
S_{Pi}	sensitivity for the ith parameter defined by (25)
S_{si}	specific storage where i = 1 for regions 1 and 2 for region 2
V_1, V_2	volumes bounded by the upper boundary and its approximate form of step change in reservoir thickness as shown in Fig. 1
V_3, V_4	volumes bounded by the lower boundary and its approximate form of step change in reservoir thickness as shown in Fig. 1
Y_0	modified Bessel function of the second kind of order zero
Y_1	modified Bessel function of the second kind of order one
α_1	$\sqrt{\kappa_{z1}}m\pi/\sqrt{\kappa_{r1}}z_1$
α_2	$\sqrt{\kappa_{z2}}m\pi/\sqrt{\kappa_{r2}}z_2$
β_1	$m\pi/z_1$
β_2	$n\pi/z_2$
χ_0	function of I_0 and K_0 defined by (15)
χ_1	function of I_0, I_1, K_0 and K_1 defined by (B5)
κ_{zi}	vertical hydraulic conductivities where i = 1 for region 1 and 2 for region 2
κ_{ri}	radial hydraulic conductivities where i = 1 for region 1 and 2 for region 2
μ_0	function of I_0 and K_0 defined by (16)
μ_1	function of I_0, I_1, K_0 and K_1 defined by (B6)
σ_0	function of K_0 defined by (18)
σ_1	function of K_0 and K_1 defined by (B7)
ς_i	$\sqrt{pS_{si}/\kappa_{ri}}$ where i = 1 for region 1 and 2 for region 2
τ_0	function of I_0 and K_0 defined by (17)
τ_1	function of I_0, I_1, K_0 and K_1 defined by (B8)
ω_0	function of K_0 defined by (19)
ω_1	function of K_0 and K_1 defined by (B9)
ξ_m, η_n	constants defined by (B4)
Δ_1	trap height of the lower boundary of a dome reservoir
Δ_2	trap height of the upper boundary of a dome reservoir
Φ	function of J_0, J_1, Y_0 and Y_1 defined by (21)
Λ	function of J_0, J_1, Y_0 and Y_1 defined by (22)
Π	function of J_0, J_1, Y_0 and Y_1 defined by (23)
Ω	function of J_0, J_1, Y_0 and Y_1 defined by (24)

based on Darcy's law and Bromwich integral method [11]. The spatial head distributions at two different times are plotted to investigate the influence of convex-upward boundaries when compared with those of the horizontal reservoir. The effects of the trap width and thickness of dome reservoir on the injection rate are also examined. In addition, the sensitivity analysis for studying the influence of the change of hydraulic conductivity or specific storage coefficient on the injection rate is performed.

2. Mathematical model

2.1. Conceptual model

Fig. 1 shows a schematic representation for an injection well with a radius of r_w located at the center of a dome reservoir with a convex-upward bend. The origin of the coordinate passes through the center of the dome structure. The upper and lower curved boundaries of the dome represented by solid lines are approximated by the form of step change denoted as dashed lines shown in Fig. 1. The volume V_1 between the dashed line and solid line should be equal to V_3. Similarly, V_2 should equal V_4. The Δ_1 and Δ_2 represent the trap heights of the lower and upper boundaries of the dome, respectively. The reservoir is divided into two regions, i.e., regions 1 and 2, with different hydraulic properties produced due to regional compression. The r_1 is the trap width measured from the center of the injection well to the interface between regions 1 and 2. The thicknesses of the dome in regions 1 and 2 are denoted as z_1 and z_2, respectively.

The governing equations depicting transient head distributions h_i in both two regions are expressed as [12]

$$\frac{\kappa_{ri}}{r}\frac{\partial}{\partial r}\left(r\frac{\partial h_i}{\partial r}\right)+\kappa_{zi}\frac{\partial^2 h_i}{\partial z^2}=S_{si}\frac{\partial h_i}{\partial t}\quad \text{for}\quad i=1,2, \tag{1}$$

where t represents time; r and z are the variables of radial and axial coordinates, respectively; κ_{ri} and κ_{zi} denote the hydraulic conductivities in radial and z direction, respectively, for ith region; S_{si} means specific storage; and i = 1 for region 1 and 2 for region 2.

The head distribution in the dome reservoir before the injection is considered as uniform. Therefore the initial condition is expressed as

$$h_i(r,z,0)=0\quad \text{for}\quad i=1,2. \tag{2}$$

The head at the wellbore is kept constant as h_w and thus the boundary condition at $r = r_w$ is expressed as

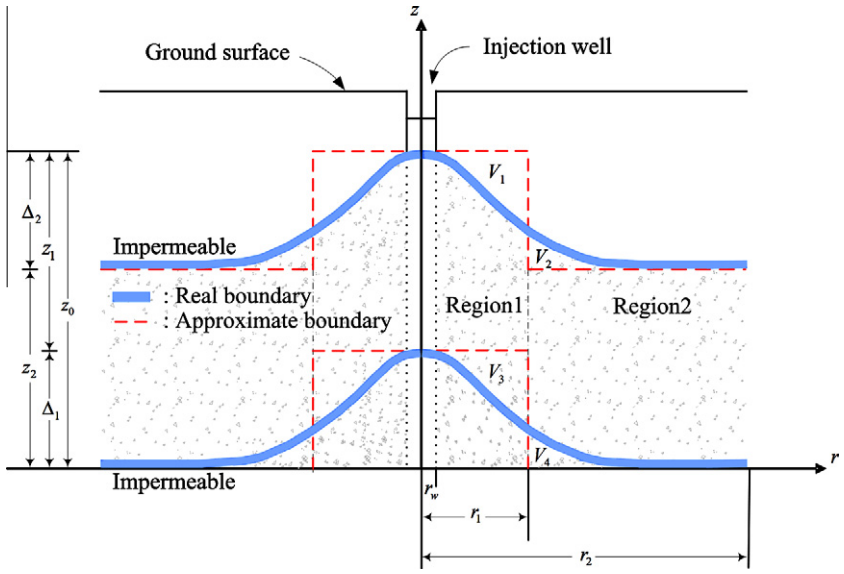

Fig. 1. Schematic representation of a dome reservoir with dual convex-upward boundaries.

$$h_1(r_w,z,t)=h_w \quad \text{for} \quad \Delta_1 \leqslant z \leqslant z_0. \tag{3}$$

The remote boundary is

$$h_2(\infty,z,t)=0 \quad \text{for} \quad 0 \leqslant z \leqslant z_2, \tag{4}$$

implying that the head is not affected by the injection.

The upper boundary of the reservoir is impermeable and thus the related boundary conditions are expressed as:

$$\frac{\partial h_1(r,z_0,t)}{\partial z}=0 \quad \text{for} \quad r_w \leqslant r \leqslant r_1 \tag{5}$$

and

$$\frac{\partial h_2(r,z_2,t)}{\partial z}=0 \quad \text{for} \quad r_1 \leqslant r \leqslant \infty. \tag{6}$$

Similarly, the lower boundary conditions for the dome reservoir are expressed as:

$$\frac{\partial h_1(r,\Delta_1,t)}{\partial z}=0 \quad \text{for} \quad r_w \leqslant r \leqslant r_1 \tag{7}$$

and

$$\frac{\partial h_2(r,0,t)}{\partial z}=0 \quad \text{for} \quad r_1 \leqslant r \leqslant \infty. \tag{8}$$

Two no-flow conditions due to the step form approximation to the upper and lower boundaries at $r = r_1$ are necessary and listed as follows.

$$\frac{\partial h_1(r_1,z,t)}{\partial r}=0 \quad \text{for} \quad z_2 \leqslant z \leqslant z_0 \tag{9}$$

and

$$\frac{\partial h_2(r_1,z,t)}{\partial r}=0 \quad \text{for} \quad 0 \leqslant z \leqslant \Delta_1. \tag{10}$$

In addition, two continuity conditions are required at $r = r_1$. One is the continuity of the head expressed as

$$h_1(r_1,z,t)=h_2(r_1,z,t) \quad \text{for} \quad \Delta_1 \leqslant z \leqslant z_2, \tag{11}$$

while the other is the continuity of the flux written as

$$\kappa_{r1}\frac{\partial h_1(r_1,z,t)}{\partial r}=\kappa_{r2}\frac{\partial h_2(r_1,z,t)}{\partial r} \quad \text{for} \quad \Delta_1 \leqslant z \leqslant z_2. \tag{12}$$

It is noted that the approximation of the upper and lower curved boundaries of the dome by the forms of step change introduces four conditions required at the interface between regions 1 and 2 as Eqs. (9)–(12).

2.2. Laplace-domain solutions for head distributions

The Laplace-domain solutions for the head distributions in both regions, $\bar{h}_1$ and $\bar{h}_2$, can be obtained by applying Laplace transform, separation of variables, and Fourier series to Eqs. (1)–(12) and the results can be written as

$$\bar{h}_1=\frac{h_w}{p}\chi_0(\varsigma_1 r)-a_0\mu_0(\varsigma_1 r)-\sum_m a_m\tau_0\left(\sqrt{\varsigma_1^2+\alpha_1^2}r\right)\cos[\beta_1(z-\Delta_1)] \tag{13}$$

and

$$\bar{h}_2=-a_0\sigma_0(\varsigma_2 r)-\sum_n b_n\omega_0\left(\sqrt{\varsigma_2^2+\alpha_2^2}r\right)\cos(\beta_2 z), \tag{14}$$

where a_0, a_m, and b_n are unknown coefficients, $\varsigma_1=\sqrt{pS_{s1}/\kappa_{r1}}$, $\varsigma_2=\sqrt{pS_{s2}/\kappa_{r2}}$, $\alpha_1=\sqrt{\kappa_{z1}}m\pi/\sqrt{\kappa_{r1}}z_1$, $\alpha_2=\sqrt{\kappa_{z2}}n\pi/\sqrt{\kappa_{r2}}z_2$, $\beta_1=m\pi/z_1$, $\beta_2=n\pi/z_2$; m and n are positive integers (i.e., 1,2,3,…); χ_0, μ_0, τ_0, σ_0 and ω_0 are lumped parameters, respectively defined as

$$\chi_0(\varsigma_1 r)=\frac{K_0(\varsigma_1 r)I_0(\varsigma_1 r_1)-I_0(\varsigma_1 r)K_0(\varsigma_1 r_1)}{K_0(\varsigma_1 r_w)I_0(\varsigma_1 r_1)-I_0(\varsigma_1 r_w)K_0(\varsigma_1 r_1)}, \tag{15}$$

$$\mu_0(\varsigma_1 r)=\frac{K_0(\varsigma_1 r)I_0(\varsigma_1 r_w)-I_0(\varsigma_1 r)K_0(\varsigma_1 r_w)}{K_0(\varsigma_1 r_1)I_0(\varsigma_1 r_w)-I_0(\varsigma_1 r_1)K_0(\varsigma_1 r_w)}, \tag{16}$$

$$\tau_0(\varsigma_1 r)=\frac{K_0\left(\sqrt{\varsigma_1^2+\alpha_1^2}r\right)I_0\left(\sqrt{\varsigma_1^2+\alpha_1^2}r_w\right)-I_0\left(\sqrt{\varsigma_1^2+\alpha_1^2}r\right)K_0\left(\sqrt{\varsigma_1^2+\alpha_1^2}r_w\right)}{K_0\left(\sqrt{\varsigma_1^2+\alpha_1^2}r_1\right)I_0\left(\sqrt{\varsigma_1^2+\alpha_1^2}r_w\right)-I_0\left(\sqrt{\varsigma_1^2+\alpha_1^2}r_1\right)K_0\left(\sqrt{\varsigma_1^2+\alpha_1^2}r_w\right)}, \tag{17}$$

$$\sigma_0(\varsigma_2 r)=\frac{K_0(\varsigma_2 r)}{K_0(\varsigma_2 r_1)} \tag{18}$$

and

$$\omega_0(\varsigma_2 r) = \frac{K_0\left(\sqrt{\varsigma_2^2 + \alpha_2^2} r\right)}{K_0\left(\sqrt{\varsigma_2^2 + \alpha_2^2} r_1\right)}, \tag{19}$$

in which I_0 and K_0 are the modified Bessel functions of the first and second kinds with order zero, respectively. The detailed development for the solutions of Eqs. (13) and (14) is presented in Appendix A. In addition, the determination of coefficients a_0, a_m and b_n in Eqs. (13) and (14) is shown in Appendix B.

2.3. Time-domain solution for injection rate

Applying Darcy's law to Eq. (13) and using the Bromwich integral method [11] to the result yields the solution for the injection rate. Note that the application of the Bromwich integral method for the Laplace-domain solution to find the time-domain solution can be seen, for example, in Yang and Yeh 2002 [13]. A detailed procedure for deriving the time-domain solution is given in Appendix C and the result is

$$Q_w(t) = 4\kappa_{r1} r_w z_1 h_w \int_0^\infty \frac{\Lambda \cdot \Pi - \Phi \cdot \Omega}{\Phi^2 + \Lambda^2} e^{-\frac{\kappa_{r1} u^2}{S_{s1}} t} du \tag{20}$$

with

$$\Phi = (z_2 - z_1) J_0(ur_1) J_1(ur_1) Y_0(ur_w) + J_0(ur_w)[z_1 J_0(ur_1) Y_1(ur_1) - z_2 J_1(ur_1) Y_0(ur_1)], \tag{21}$$

$$\Lambda = [(z_1 - z_2) J_0(ur_w) Y_0(ur_1) + z_2 J_0(ur_1) Y_0(ur_w)] Y_1(ur_1) - z_1 J_1(ur_1) Y_0(ur_1) Y_0(ur_w), \tag{22}$$

$$\Pi = [z_2 J_1(ur_w) Y_0(ur_1) + (z_1 - z_2) J_0(ur_1) Y_1(ur_w)] J_1(ur_1) - z_1 J_0(ur_1) J_1(ur_w) Y_1(ur_1), \tag{23}$$

$$\Omega = (z_2 - z_1) J_1(ur_w) Y_0(ur_1) Y_1(ur_1) + z_1 J_1(ur_1) Y_0(ur_1) - z_2 J_0(ur_1) Y_1(ur_1) Y_1(ur_w), \tag{24}$$

where u is a dummy variable for the integration; J_0 and Y_0 are the modified Bessel functions of the first and second kinds with order zero, respectively; J_1 and Y_1 are the modified Bessel functions of the first and second kinds with order one, respectively. It is noteworthy that the injection rate is proportional to h_w according to Eq. (20).

2.4. Sensitivity analysis

The sensitivity analysis is performed herein to investigate the change of injection rate in response to the change of aquifer parameter or dome geometry. The sensitivity of the wellbore flow rate to a specific parameter can be expressed as

$$S_{Pi} = \frac{\partial Q_w}{\partial P_i}, \tag{25}$$

where P_i represents the ith parameter in Eq. (20). A dimensionless form of the sensitivity may be written as [14]

$$S_{i,t} = \frac{\partial Q_w / Q_w}{\partial P_i / P_i}, \tag{26}$$

where $S_{i,t}$ is the normalized sensitivity coefficient at time t for the ith parameter.

3. Results and discussion

Following sections present the investigations of the head distribution near the location of step change, the effect of geometry of the dome reservoir, and the sensitivity analysis for the injection rate in regard to the aquifer parameters and the heights of dome reservoir. The dome reservoir is considered to be homogeneous and isotropic (i.e.,$\kappa_{r1} = \kappa_{r2} = \kappa_r$, $\kappa_{z1} = \kappa_{z2} = \kappa_z$ and $S_{s1} = S_{s2} = S_s$) in this study. The issue regarding the effect of aquifer heterogeneity or anisotropy of an anticline on the head distribution can be referred to the work of Yeh and Kuo [9]. The hydraulic conductivity and specific storage are assumed to be 1 m/day and 10^{-5} m^{-1}, respectively. The thicknesses of this reservoir for both regions are chosen as 40 m. The trap width is 100 m and both trap heights for the lower and upper boundary are 10 m. The fully penetrating well has the radius of 0.2 m. The head at the wellbore is considered to be 50 m which equals 9.36 Mpa under a normal condition of CO_2 injection [9].

3.1. Spatial and temporal head distribution

The head distribution in time domain can be obtained based on Eqs. (13) and (14) and Stehfest algorithm [12,10]. Fig. 2(a) shows the simulation results of spatial head distribution at $t = 30$ and 365 days for $r_w = 0.2$ m, $r_1 = 100$ m, $z_0 = 50$ m, $z_1 = z_2 = 40$ m, $h_w = 50$ m, $\kappa_r = \kappa_z = 1$ m/day and $S_s = 10^{-5}$ m^{-1}. Note that this is a homogeneous and isotropic case when applying the present solution developed for heterogeneous and anisotropic media. The contours of the head distribution are vertical and the flow is horizontal in the reservoir except near the spot of step change where some significant vertical flow components can be observed. In contrast, Fig. 2(b) indicates that the flow is all horizontal for the flat aquifer and its flow velocity is slightly higher than that in the dome reservoir.

3.2. Effect of reservoir geometry on injection rate

This section investigates the effects of the trap width and thickness of dome on the injection rate. Fig. 3 presents the temporal injection rate for $r_w = 0.2$ m, $h_w = 50$ m, $\kappa_r = 1$ m/day, $S_s = 10^{-5}$ m^{-1} for r_1 at 100 m and 2000 m and $z_1 = z_2$ of 40 m and 45 m. The figure shows that the injection rates decreases with increasing time. For $r_1 = 100$ m, the dome with a larger z_1 has a larger injection rate than that with a smaller z_1. This is because the thicker dome has a larger volume to store the injected fluid. In addition, for $z_1 = z_2$ of 40 m, the curves of injection rate are the same, indicating that the location of r_1 has no effect on the injection rate if the dome volume is fixed.

The effects of different thicknesses in regions 1 and 2 on injection rate are examined. Fig. 4 shows the temporal injection rate for various values of z_1 and z_2. For the same z_2 of 20 m or 40 m, the dome with a larger z_1 has significantly larger injection rate than that with a smaller z_1. However, for the same z_1 of 20 m or 40 m, the differences of injection rate are very small. Such a result indicates that z_1 is a more important parameter than z_2 in storing the injected fluid.

Fig. 5 displays the temporal injection rate per unit thickness (Q/z_1) for the cases that $r_1 = 100$ m and 2000 m with $z_1/z_2 = 0.5$, 1, and 2. The values of Q/z_1 for different values of z_1/z_2 are almost identical before $t = 0.02$ days for $r_1 = 100$ m, indicating the domes with the same z_1 but different z_2 have the same injection rate Q before that time. After $t = 0.02$ days, the curve with a smaller z_1/z_2 has a larger Q/z_1 reflecting that a dome with a larger z_2 has larger capacity than that with a smaller z_2 to store more injected fluid after

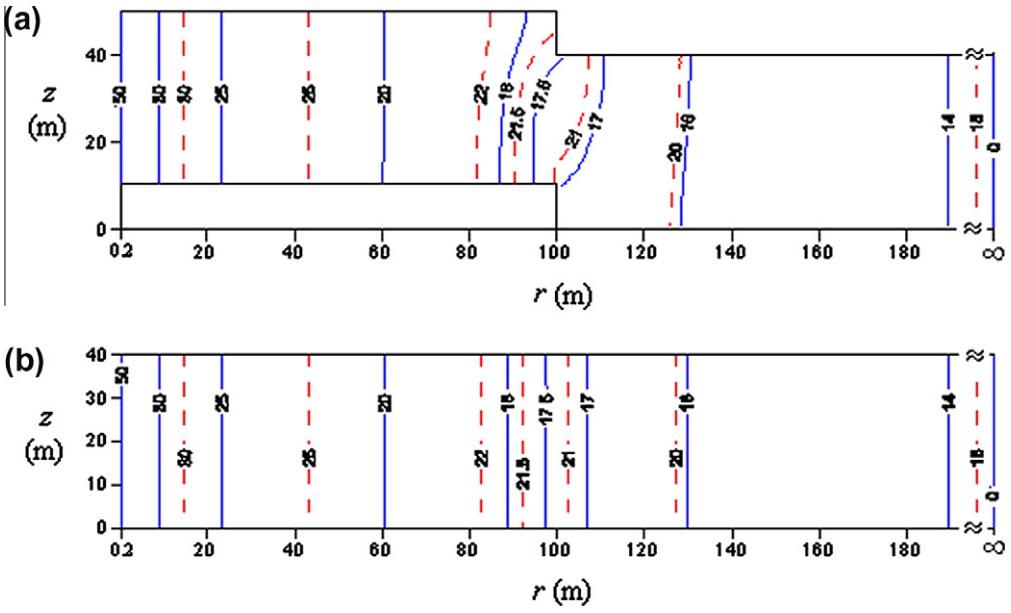

Fig. 2. Spatial head distribution for (a) a dome reservoir and (b) a horizontal reservoir with $r_w = 0.2$ m, $r_1 = 100$ m, $z_1 = z_2 = 40$ m, $h_w = 50$ m, $\kappa_r = 1$ m/day and $S_s = 10^{-5}$ m^{-1} at $t = 30$ days (solid lines) and $t = 365$ days (dashed lines).

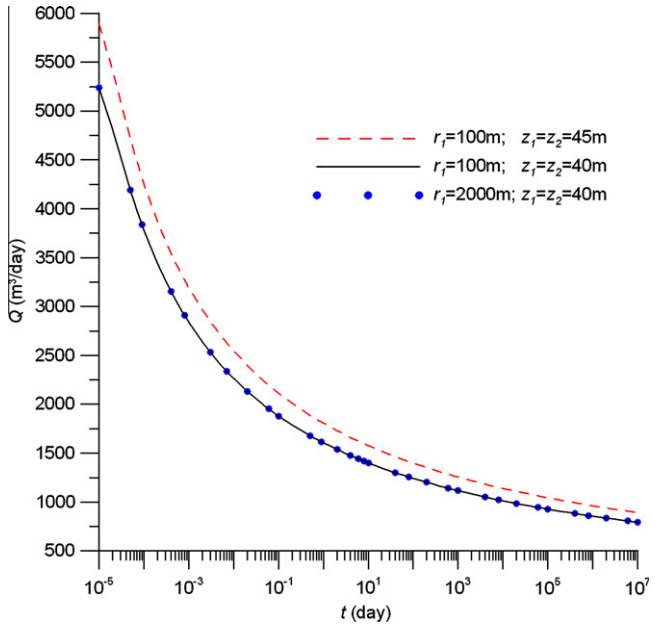

Fig. 3. Temporal injection rate for $r_w = 0.2$ m, $s_w = 50$ m, $\kappa_r = 1$ m/day, $S_s = 10^{-5}$ m^{-1} with $r_1 = 100$ m and 2000 m when $z_1 = z_2$.

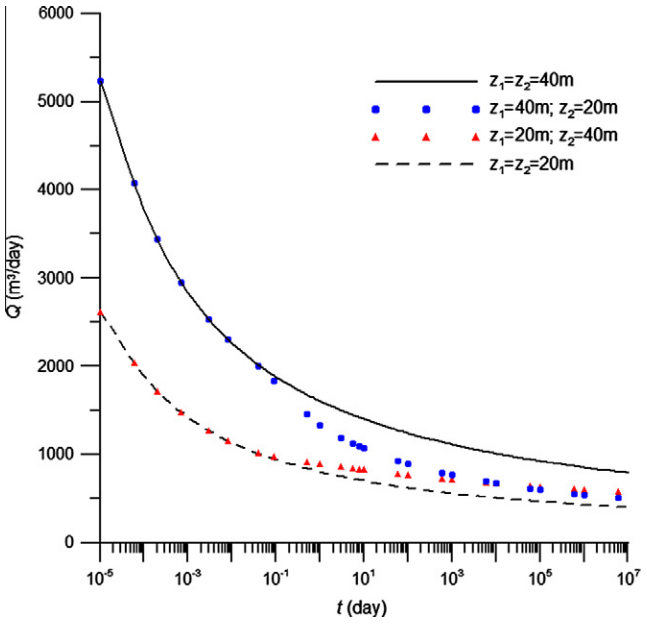

Fig. 4. Temporal injection rate for $r_w = 0.2$ m, $s_w = 50$ m, $\kappa_r = 1$ m/day, $S_s = 10^{-5}$ m^{-1}, $r_1 = 100$ m with z_1 and $z_2 = 20$ m and 40 m.

$t = 0.02$ days. Similarly, the values of Q/z_1 for different values of z_1/z_2 are almost identical before $t = 10$ days and start to deviate from each other after that time for $r_1 = 2000$ m. Physically, those results indicate the injected fluid reaches the interface between regions 1 and 2 at time of 0.02 days for $r_1 = 100$ m and at time of 10 days for $r_1 = 2000$ m. Note that the data for the case that $r_1 = 2000$ m are taken form Li [15] for a salt dome in the Gulf of Mexico.

3.3. Sensitivity analysis

In this section, sensitivity analysis is performed to examine the responses of injection rate to the relative changes in various parameters. Fig. 6 shows the temporal normalized sensitivity coefficient of the injection rate evaluated by Eq. (26) to the parameters κ_r, S_s, z_1 and z_2 for $r_1 = 100$ m and 2000 m. The figure shows that z_1, the thickness of the dome (region 1), is the most sensitive parameter at the very early period of injection. Within this period, the relative change in injection is exactly equal to the relative change in z_1, indicating that z_1 is the dominate and most important parameter at early injection time. After about 0.1 days, the normalized sensitivity coefficient for κ_r becomes the largest all the time, indicating that the injection rate is the most sensitive to the relative change in κ_r among those parameters. In contrast, the injection rate is almost insensitive to the relative change in S_s because of its small normalized sensitivity coefficient. Naturally, the S_s therefore allows higher degree of uncertainty in estimation. It is

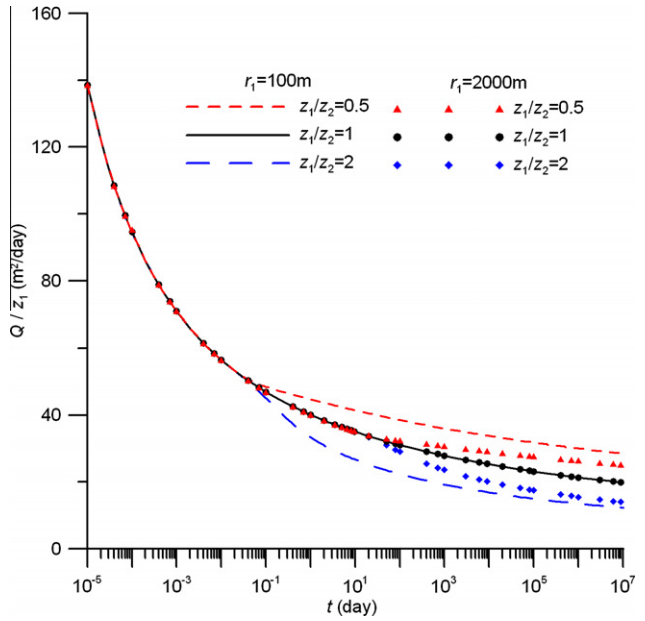

Fig. 5. Temporal injection rate per unit thickness z_1 for $r_w = 0.2$ m, $s_w = 50$ m, $\kappa_r = 1$ m/day, $S_s = 10^{-5}$ m^{-1} with $z_1/z_2 = 0.5$, 1, and 2 when $r_1 = 100$ m and 2000 m.

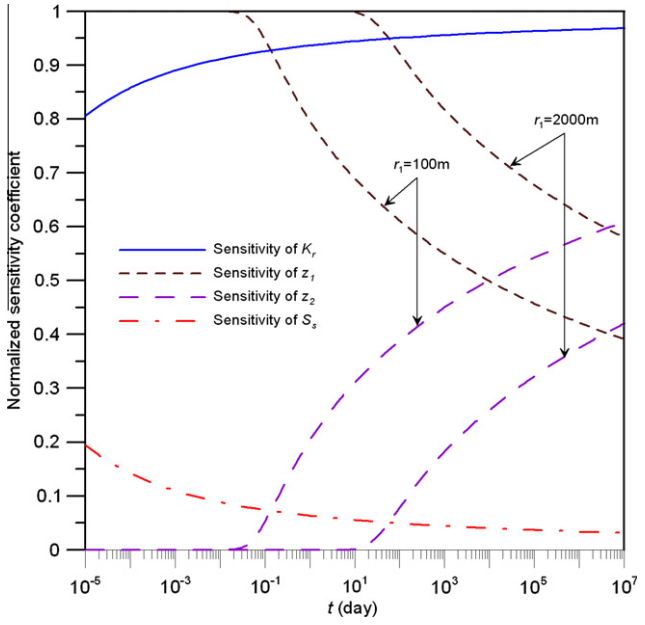

Fig. 6. The temporal normalized sensitivity coefficients of the parameters κ_r, S_s, z_1 and z_2 for $r_1 = 100$ m and 2000 m.

worth noting that the normalized sensitivity of S_s is high at very early time of injection and gradually declines and finally approaches a constant. Such a high sensitivity of S_s reflects the elastic behavior of aquifers instantaneously in response to the injection.

It is interesting to note that, for $r_1 = 100$ m, the normalized sensitivity coefficient to z_1 starts to decrease but the one to z_2 begins to increase when $t = 0.02$ days. This result indicates that the effect of z_1 on the injection rate is very short and quickly decreases as time progresses. However, the impact of z_1 on the injection rate is still strong until the time reaches 10^4 days. One can observe that the sensitivity coefficient curves for z_1 and z_2 crisscross at $t = 10^4$ days, indicating that the injection rate is more sensitive to the relative change of z_2 than that of z_1 afterward. On the other hand, the curves of normalized sensitivity coefficients to the parameters z_1 and z_2 for $r_1 = 2000$ m occurring after t=10 days have similar patterns to those of the case for $r_1 = 100$ m. Obviously, a larger value of r_1 delays the response time of the injection rate to the relative changes of z_1 and z_2. Interestingly, Fig. 6 also reveals that the injected fluid arrives at the interface between regions 1 and 2 near the time of 0.02 days for $r_1 = 100$ m and about 10 days for 2000 m.

4. Concluding remarks

A new mathematical model is developed for describing spatial head distribution in a heterogeneous and anisotropic dome reservoir. A form of step change is adopted to approximate the shape of dome reservoirs with dual convex-upward boundaries. The semi-analytical solution of head distribution is derived by Fourier series and Laplace transform. Then, the time-domain results for the head distribution are evaluated by Stehfest algorithm and the time-domain solution for the injection rate at wellbore is developed based on Darcy's law and the Bromwich integral method. The effects of geometry of reservoir and hydraulic parameters on the injection rate are investigated. The present solutions can be applied to assess the capacity of fluid storage in dome reservoirs. Several conclusions shown below can be drawn from this study.

1. A transient flow field in a dome reservoir is produced after the start of injection. The flow has a vertical component near the step change while the flow is horizontal for the region far away from the change. In addition, the flow velocity in a horizontal reservoir is slightly higher than that in the dome reservoir.
2. The thickness of dome reservoir has a significant effect on the injection rate because of much storage while the location of step change has no effect on the injection rate due to a fixed reservoir volume. It also indicates that the thickness of the convex-upward structure of a dome is a more important parameter than that of horizontal structure in storing the injected fluid.
3. The temporal injection rate per unit thickness for various reservoir geometries is dominated strongly by the trap width. As increasing the trap width, the time-lag effect on injected fluid in progress to escape from the trap region of a dome is enlarged.
4. The results of normalized sensitivity analysis indicate that the injection rate is the most sensitive to the relative change in hydraulic conductivity and the least sensitive to the relative change in specific storage after a short period of injection time. On the other hand, it is necessary for marking a higher sensitivity of S_s at very early time of injection because this reveals the elastic mechanics in aquifers instantaneously owing to the injection.

Acknowledgements

Research leading to this work has been partially supported by the Grants from Taiwan National Science Council under the contract numbers NSC 99-NU-E-009-001 and NSC 99-2221-E-009-062-MY3.

Appendix A. Development for head solutions of Eqs. (13) and (14)

Applying Laplace transform to Eqs. (1)–(12) results in the flow equation and associated boundary and continuity conditions in terms of r and z as

$$\frac{\kappa_{ri}}{r}\frac{\partial}{\partial r}\left(r\frac{\partial \bar{h}_i}{\partial r}\right)+\kappa_{zi}\frac{\partial^2 \bar{h}_i}{\partial z^2}=S_s p\bar{h}_i \quad \text{for} \quad i=1,2, \tag{A1}$$

$$\bar{h}_1(r_w,z,p)=\frac{h_w}{p} \quad \text{for} \quad \Delta_1 \leqslant z \leqslant z_0, \tag{A2}$$

$$\bar{h}_2(\infty,z,p)=0 \quad \text{for} \quad 0 \leqslant z \leqslant z_2, \tag{A3}$$

$$\frac{\partial \bar{h}_1(r,z_0,p)}{\partial z}=0 \quad \text{for} \quad r_w \leqslant r \leqslant r_1, \tag{A4}$$

$$\frac{\partial \bar{h}_1(r_1,z,p)}{\partial r}=0 \quad \text{for} \quad z_2 \leqslant z \leqslant z_0, \tag{A5}$$

$$\frac{\partial \bar{h}_2(r,z_2,p)}{\partial z}=0 \quad \text{for} \quad r_1 \leqslant r \leqslant \infty, \tag{A6}$$

$$\frac{\partial \bar{h}_1(r,\Delta_1,p)}{\partial z}=0 \quad \text{for} \quad r_w \leqslant r \leqslant r_1, \tag{A7}$$

$$\frac{\partial \bar{h}_2(r_1,z,p)}{\partial r}=0 \quad \text{for} \quad 0 \leqslant z \leqslant \Delta_1, \tag{A8}$$

$$\frac{\partial \bar{h}_2(r,0,p)}{\partial z}=0 \quad \text{for} \quad r_1 \leqslant r \leqslant \infty, \tag{A9}$$

$$\bar{h}_1(r_1,z,p)=\bar{h}_2(r_1,z,p) \quad \text{for} \quad \Delta_1 \leqslant z \leqslant z_2, \tag{A10}$$

$$\kappa_{r1}\frac{\partial \bar{h}_1(r_1,z,p)}{\partial r}=\kappa_{r2}\frac{\partial \bar{h}_2(r_1,z,p)}{\partial r} \quad \text{for} \quad \Delta_1 \leqslant z \leqslant z_2. \tag{A11}$$

The solution of Eq. (A1) in Laplace domain for $i = 1$ after applying the method of separation of variables with Eqs. (A4) and (A7) is

$$\bar{h}_1 = E_0 I_0(\varsigma_1 r)+F_0 K_0(\varsigma_1 r) + \sum_m \left[E_m I_0\left(\sqrt{\varsigma_1^2+\alpha_1^2}r\right)+F_m K_0\left(\sqrt{\varsigma_1^2+\alpha_1^2}r\right)\right]\cos[\beta_1(z-\Delta_1)], \tag{A12}$$

where E_0, F_0, E_m and F_m are unknown coefficients. Substituting Eq. (A12) into (A2) leads to

$$\frac{\bar{h}_w}{p}=E_0 I_0(\varsigma_1 r_w)+F_0 K_0(\varsigma_1 r_w) + \sum_m \left[E_m I_0\left(\sqrt{\varsigma_1^2+\alpha_1^2}r_w\right)+F_m K_0\left(\sqrt{\varsigma_1^2+\alpha_1^2}r_w\right)\right]\cos[\beta_1(z-\Delta_1)]. \tag{A13}$$

The bracket term in Eq. (A13) should be zero because the left-hand side of Eq. (A13) is independent of z. That is

$$E_m I_0\left(\sqrt{\varsigma_1^2+\alpha_1^2}r_w\right)+F_m K_0\left(\sqrt{\varsigma_1^2+\alpha_1^2}r_w\right)=0 \tag{A14}$$

and

$$\frac{h_w}{p}=E_0 I_0(\varsigma_1 r_w)+F_0 K_0(\varsigma_1 r_w). \tag{A15}$$

With substituting $r = r_1$ into Eq. (A12), the head at $r = r_1$ can be written as

$$\bar{\Psi}(z)=E_0 I_0(\varsigma_1 r_1)+F_0 K_0(\varsigma_1 r_1) + \sum_m \left[E_m I_0\left(\sqrt{\varsigma_1^2+\alpha_1^2}r_1\right)+F_m K_0\left(\sqrt{\varsigma_1^2+\alpha_1^2}r_1\right)\right]\cos[\beta_1(z-\Delta_1)]. \tag{A16}$$

The bracket term in Eq. (A16) is represented by an unknown constant, a_m, as

$$a_m=-\left[E_m I_0\left(\sqrt{\varsigma_1^2+\alpha_1^2}r_1\right)+F_m K_0\left(\sqrt{\varsigma_1^2+\alpha_1^2}r_1\right)\right]. \tag{A17}$$

A coefficient of Fourier series determined by integrating Eq. (A16) with respect to z from zero to z_0 can be obtained as [16]

$$a_0=-\frac{1}{z_0}\int_0^{z_0}\bar{\Psi}(z)\,dz=-[E_0 I_0(\varsigma_1 r_1)+F_0 K_0(\varsigma_1 r_1)]. \tag{A18}$$

Note that the result of integration for the last term of Eq. (A16) is zero.

The constants E_0 and F_0 can be gotten from solving Eqs. (A15) and (A18) as

$$E_0=\frac{(h_w/p)K_0(\varsigma_1 r_1)+a_0 K_0(\varsigma_1 r_w)}{K_0(\varsigma_1 r_1)I_0(\varsigma_1 r_w)-I_0(\varsigma_1 r_1)K_0(\varsigma_1 r_w)} \tag{A19}$$

and

$$F_0=\frac{(h_w/p)I_0(\varsigma_1 r_1)+a_0 I_0(\varsigma_1 r_w)}{K_0(\varsigma_1 r_w)I_0(\varsigma_1 r_1)-I_0(\varsigma_1 r_w)K_0(\varsigma_1 r_1)}. \tag{A20}$$

Moreover, the constants E_m and F_m are solved from Eqs. (A14) and (A17) as

$$E_m=\frac{a_m K_0\left(\sqrt{\varsigma_1^2+\alpha_1^2}r_w\right)}{K_0\left(\sqrt{\varsigma_1^2+\alpha_1^2}r_1\right)I_0\left(\sqrt{\varsigma_1^2+\alpha_1^2}r_w\right)-I_0\left(\sqrt{\varsigma_1^2+\alpha_1^2}r_1\right)K_0\left(\sqrt{\varsigma_1^2+\alpha_1^2}r_w\right)} \tag{A21}$$

and

$$F_m=\frac{-a_m I_0\left(\sqrt{\varsigma_1^2+\alpha_1^2}r_w\right)}{K_0\left(\sqrt{\varsigma_1^2+\alpha_1^2}r_1\right)I_0\left(\sqrt{\varsigma_1^2+\alpha_1^2}r_w\right)-I_0\left(\sqrt{\varsigma_1^2+\alpha_1^2}r_1\right)K_0\left(\sqrt{\varsigma_1^2+\alpha_1^2}r_w\right)}. \tag{A22}$$

Substituting Eqs. (A19)–(A22) into Eq. (A12) leads to Eq. (13).

Similarly, the solution of Eq. (A1) for $i = 2$ in Laplace domain with Eqs. (A6) and (A9) can be obtained as

$$\bar{h}_2 = \bar{E}_0 I_0(\varsigma_2 r)+\bar{F}_0 K_0(\varsigma_2 r) + \sum_n \left[E_n I_0\left(\sqrt{\varsigma_2^2+\alpha_2^2}r\right)+F_n K_0\left(\sqrt{\varsigma_2^2+\alpha_2^2}r\right)\right]\cos(\beta_2 z), \tag{A23}$$

where $\bar{E}_0$, $\bar{F}_0$, E_n and F_n are unknown coefficients. Both $\bar{E}_0$ and E_n should be zero due to the remote boundary condition Eq. (A3). Eq. (A23) is therefore written as

$$\bar{h}_2=\bar{F}_0 K_0(\varsigma_2 r)+\sum_n F_n K_0\left(\sqrt{\varsigma_2^2+\alpha_2^2}r\right)\cos(\beta_2 z). \tag{A24}$$

Let $r = r_1$ in Eq. (A24), the head at $r = r_1$ can then be expressed as

$$\bar{\Psi}(z)=\bar{F}_0 K_0(\varsigma_2 r_1)+\sum_n F_n K_0\left(\sqrt{\varsigma_2^2+\alpha_2^2}r_1\right)\cos(\beta_2 z). \tag{A25}$$

According to the determination of a coefficient of Fourier series, one can get

$$a_0=-\frac{1}{z_0}\int_0^{z_0}\Psi(z)dz=-\bar{F}_0 K_0(\varsigma_2 r_1). \tag{A26}$$

Thus, one can obtain

$$\bar{F}_0=-a_0/K_0(\varsigma_2 r_1). \tag{A27}$$

Assume that $b_n=-F_n K_0\left(\sqrt{\varsigma_2^2+\alpha_2^2}r_1\right)$. Thus, one can write

$$F_n=-b_n/K_0\left(\sqrt{\varsigma_2^2+\alpha_2^2}r_1\right). \tag{A28}$$

Finally, Eq. (14) can be obtained after substituting Eqs. (A27) and (A28) into Eq. (A24).

Appendix B. Evaluation of coefficients a_0, a_m and b_n

The unknowns a_0 and a_m can be obtained based on the boundary conditions (Eqs. (A5) and (A8)) as well as the requirement of continuity of flux (Eq. (A11)). Substituting Eq. (13) into Eq. (A8) results in

$$\tilde{c}_3 a_0 + \sum_n b_n \eta_n \cos(\beta_2 z) = 0 \quad \text{for} \quad 0 \leqslant z \leqslant \Delta_1. \tag{B1}$$

Substituting Eqs. (13) and (14) into Eq. (A11) gives

$$-\tilde{c}_1 \frac{h_w}{p} + \tilde{c}_2 a_0 + \sum_m a_m \xi_m \cos[\beta_1 (z - \Delta_1)] = \tilde{c}_3 a_0 + \sum_n b_n \eta_n \cos(\beta_2 z) \quad \text{for} \quad \Delta_1 \leqslant z \leqslant z_2. \tag{B2}$$

Placing Eq. (14) in Eq. (A5) leads to

$$-\tilde{c}_1 \frac{h_w}{p} + \tilde{c}_2 a_0 + \sum_m a_m \xi_m \cos[\beta_1 (z - \Delta_1)] = 0 \quad \text{for} \quad z_2 \leqslant z \leqslant z_0 \tag{B3}$$

with

$$\tilde{c}_1 = \varsigma_1 \chi_1(\varsigma_1 r_1), \quad \tilde{c}_2 = \varsigma_1 \mu_1(\varsigma_1 r_1), \quad \tilde{c}_3 = \varsigma_2 \sigma_1(\varsigma_2 r_1),$$
$$\xi_m = \sqrt{\varsigma_1^2 + \alpha_1^2}\, \tau_1\left(\sqrt{\varsigma_1^2 + \alpha_1^2} r_1\right), \quad \eta_n = \sqrt{\varsigma_2^2 + \alpha_2^2}\, \omega_1\left(\sqrt{\varsigma_2^2 + \alpha_2^2} r_1\right), \tag{B4}$$

$$\chi_1(\varsigma_1 r_1) = \frac{K_1(\varsigma_1 r_1) I_0(\varsigma_1 r_1) + I_1(\varsigma_1 r_1) K_0(\varsigma_1 r_1)}{K_0(\varsigma_1 r_w) I_0(\varsigma_1 r_1) - I_0(\varsigma_1 r_w) K_0(\varsigma_1 r_1)}, \tag{B5}$$

$$\mu_1(\varsigma_1 r_1) = \frac{K_1(\varsigma_1 r_1) I_0(\varsigma_1 r_w) + I_1(\varsigma_1 r_1) K_0(\varsigma_1 r_w)}{K_0(\varsigma_1 r_1) I_0(\varsigma_1 r_w) - I_0(\varsigma_1 r_1) K_0(\varsigma_1 r_w)}, \tag{B6}$$

$$\sigma_1(\varsigma_2 r_1) = \frac{K_1(\varsigma_2 r_1)}{K_0(\varsigma_2 r_1)}, \tag{B7}$$

$$\tau_1(\varsigma_1 r_1) = \frac{K_1\left(\sqrt{\varsigma_1^2 + \alpha_1^2} r_1\right) I_0\left(\sqrt{\varsigma_1^2 + \alpha_1^2} r_w\right) + I_1\left(\sqrt{\varsigma_1^2 + \alpha_1^2} r_1\right) K_0\left(\sqrt{\varsigma_1^2 + \alpha_1^2} r_w\right)}{K_0\left(\sqrt{\varsigma_1^2 + \alpha_1^2} r_1\right) I_0\left(\sqrt{\varsigma_1^2 + \alpha_1^2} r_w\right) - I_0\left(\sqrt{\varsigma_1^2 + \alpha_1^2} r_1\right) K_0\left(\sqrt{\varsigma_1^2 + \alpha_1^2} r_w\right)}, \tag{B8}$$

$$\omega_1(\varsigma_2 r_1) = \frac{K_1\left(\sqrt{\varsigma_2^2 + \alpha_1^2} r_1\right)}{K_0\left(\sqrt{\varsigma_2^2 + \alpha_1^2} r_1\right)}, \tag{B9}$$

where I_1 and K_1 are the modified Bessel functions of the first and second kinds with order one, respectively. For an expression of Fourier series, adding the term $-\tilde{c}_1 \frac{h_w}{p} + \tilde{c}_2 a_0$ and $\sum_m a_m \xi_m \cos(\delta_m z)$ with $\delta_m = m\pi / z_0$ to both sides of Eq. (B1) yields

$$-\tilde{c}_1 \frac{h_w}{p} + (\tilde{c}_2 + \tilde{c}_3) a_0 + \sum_n b_n \eta_n \cos(\beta_2 z) + \sum_m a_m \xi_m \cos(\delta_m z) = \left(-\tilde{c}_1 \frac{h_w}{p} + \tilde{c}_2 a_0\right) + \sum_j a_j \xi_j \cos(\delta_j z) \quad \text{for} \quad 0 \leqslant z \leqslant \Delta_1. \tag{B10}$$

Similarly, adding the term $\sum_m a_m \xi_m \cos(\delta_m z)$ to both sides of Eqs. (B2) and (B3) results in Eqs. (B11) and (B12), respectively, as

$$\tilde{c}_3 a_0 + \sum_n b_n \eta_n \cos(\beta_2 z) + \sum_m a_m \xi_m \{\cos(\delta_m z) - \cos[\beta_1 (z - \Delta_1)]\} = \left(-\tilde{c}_1 \frac{h_w}{p} + \tilde{c}_2 a_0\right) + \sum_j a_j \xi_j \cos(\delta_j z) \quad \text{for} \quad \Delta_1 \leqslant z \leqslant z_2, \tag{B11}$$

$$\sum_m a_m \xi_m \{\cos(\delta_m z) - \cos[\beta_1 (z - \Delta_1)]\} = \left(-\tilde{c}_1 \frac{h_w}{p} + \tilde{c}_2 a_0\right) + \sum_j a_j \xi_j \cos(\delta_j z) \quad \text{for} \quad z_2 \leqslant z \leqslant z_0, \tag{B12}$$

where the subscript j is an integer from 1,2,3... The bracket terms on the left-hand side of Eqs. (B10)–(B12) represent a constant of Fourier series and $a_j \xi_j$ represents the coefficient for each $\cos(\delta_j z)$. Based on the formula of Fourier series, the unknowns a_0 and $a_j \xi_j$ can, respectively, be expressed as

$$a_0 = \frac{\tilde{c}_1 z_1}{\tilde{c}_2 z_1 - \tilde{c}_3 z_2} \frac{h_w}{p} \tag{B13}$$

and

$$a_j \xi_j = X_j a_0 - \frac{2\tilde{c}_1 \sin(\delta_j \Delta_1)}{\delta_j z_0} \frac{h_w}{p} + \sum_n \Theta_{jn} \eta_n b_n + \sum_m a_m \xi_m (E_{mj} - H_{mj}), \tag{B14}$$

where

$$X_j = \frac{2[\tilde{c}_2 \sin(\delta_j \Delta_1) + \tilde{c}_3 \sin(\delta_j z_2)]}{\delta_j z_0}, \tag{B15}$$

$$\Theta_{jn} = \frac{\sin(\beta_2 z_2 + \delta_j z_2)}{\beta_2 z_0 + \delta_j z_0} + \frac{\sin(\beta_2 z_2 - \delta_j z_2)}{\beta_2 z_0 - \delta_j z_0} \quad \text{for} \quad \beta_2 \neq \delta_j, \tag{B16}$$

$$\Theta_{jn} = \frac{z_2}{z_0} \quad \text{for} \quad \beta_2 = \delta_j, \tag{B17}$$

$$E_{mj} = 0 \quad \text{for} \quad \delta_m \neq \delta_j, \tag{B18}$$

$$E_{mj} = 1 \quad \text{for} \quad \delta_m = \delta_j, \tag{B19}$$

$$H_{mj} = \left(\frac{1}{\beta_1 - \delta_j} + \frac{1}{\beta_1 - \delta_j}\right) \frac{\sin(\delta_j \Delta_{r1})}{z_0} \quad \text{for} \quad \beta_1 \neq \delta_j, \tag{B20}$$

$$H_{mj} = \frac{z_1}{z_0} \cos(\delta_j \Delta_{r1}) \quad \text{for} \quad \beta_1 \neq \delta_j. \tag{B21}$$

Note that the value of a_j is in fact equal to a_m.

In a similar manner, the unknown b_n can be obtained based on the requirement of continuity in hydraulic head, i.e., Eq. (A10). Substituting Eqs. (13) and (14) into Eq. (A10) leads to

$$\sum_m a_m \cos[\beta_1 (z - \Delta_1)] = \sum_n b_n \cos(\beta_2 z) \quad \text{for} \quad \Delta_1 \leqslant z \leqslant z_2. \tag{B22}$$

For an expression of Fourier Series, adding $\sum_n b_n \cos(\theta_n z)$ to both sides of Eq. (B22) yields

$$\sum_m a_m \cos[\beta_1 (z - \Delta_1)] - \sum_n b_n [\cos(\beta_2 z) - \cos(\theta_n z)] = \sum_j b_j \cos(\theta_j z) \quad \text{for} \quad \Delta_1 \leqslant z \leqslant z_2, \tag{B23}$$

where $\theta_n = n\pi / (z_2 - \Delta_1)$. The unknown b_j can then be written as

$$b_j = \sum_m a_m \gamma_{mj} - \sum_n b_n (O_{nj} - P_{nj}), \tag{B24}$$

where

$$\gamma_{mj} = \frac{\sin(\beta_1 z_e + \theta_j z_e)}{\beta_1 z_e + \theta_j z_e} + \frac{\sin(\beta_1 z_e - \theta_j z_e)}{\beta_1 z_e - \theta_j z_e} \quad \text{for} \quad \beta_1 \neq \theta_j, \tag{B25}$$

$$\gamma_{mj} = 1 \quad \text{for} \quad \beta_1 = \theta_j, \tag{B26}$$

$$O_{nj} = -\left[\frac{1}{\beta_2 z_e + \theta_j z_e} + \frac{1}{\beta_2 z_e - \theta_j z_e}\right] \sin(\beta_2 \Delta_1) \quad \text{for} \quad \beta_2 \neq \theta_j, \tag{B27}$$

$$O_{nj} = \cos(\theta_j \Delta_1) - \frac{\sin(\theta_j \Delta_1)}{2\theta_j z_e} \quad \text{for} \quad \beta_2 \neq \theta_j, \tag{B28}$$

$$P_{nj} = 0 \quad \text{for} \quad \theta_n \neq \theta_j, \tag{B29}$$

$$P_{nj} = 1 \quad \text{for} \quad \theta_n = \theta_j. \tag{B30}$$

Note that b_j also equals b_n.

Eqs. (B13), (B14) and (B24) are linear with respect to the unknowns a_0, a_m and b_n. Therefore, a_m can be solved after substituting Eqs. (B13) and (B24) into (B14) and the result is

$$\sum_m Y_{jm} a_m = \lambda_j \frac{h_w}{p}, \tag{B31}$$

where

$$Y_{jm} = \xi_m \Psi_{jm} + \sum_n \overline{\Gamma}_{jn} \eta_n \Theta_{nj} \gamma_{mj}, \tag{B32}$$

$$\Psi_{jm} = E_{jm} - H_{jm} - I_{jm}, \tag{B33}$$

$$\overline{\Gamma}_{jn} = [O_{nj} - P_{nj} + I_{nj}]^{-1}, \tag{B34}$$

$$\lambda_j = \frac{2\tilde{c}_1 \sin(\delta_j \Delta_1)}{\delta_j z_0} - \frac{\tilde{c}_1 z_1}{\tilde{c}_2 z_1 - \tilde{c}_3 z_2} X_j. \tag{B35}$$

The constant b_n can be obtained after substituting a_m of Eq. (B31) into Eq. (B14).

Appendix C. Development of Eq. (20)

The Laplace-domain solution for the injection rate can be obtained based on Darcy's law as

$$Q_w = \int_{\Delta_1}^{z_0} 2\pi \kappa_{r1} r_w \left. \frac{\partial \bar{h}_1}{\partial r} \right|_{r=r_w} dz. \tag{C1}$$

With Eq. (13), the hydraulic gradient at the rim of the wellbore is expressed as

$$\left. \frac{\partial \bar{h}_1}{\partial r} \right|_{r=r_w} = a_0 \varsigma_1 \mu_1(r_w \varsigma_1) - \frac{h_w \varsigma_1 \chi_1(r_w \varsigma_1)}{p} + \sum_m a_m \times \sqrt{\varsigma_1^2 + \alpha_1^2}\, \tau_1 \left\{ r_w \sqrt{\varsigma_1^2 + \alpha_1^2} \cos[\beta_1 (z - \Delta_1)] \right\}. \tag{C2}$$

Based on Eqs. (B13) and (C2), the result of integration of Eq. (C1) yields

$$Q_w(p) = 2\pi \kappa_r r_w z_1 \varsigma_1 \times \frac{h_w}{p} \left[\frac{z_1 \varsigma_1 \chi_1(r_1 \varsigma_1) \mu_1(r_w \varsigma_1) - z_1 \varsigma_1 \chi_1(r_w \varsigma_1) \mu_1(r_1 \varsigma_1) + z_2 \varsigma_2 \sigma_1(r_1 \varsigma_2) \chi_1(r_w \varsigma_2)}{z_1 \varsigma_1 \mu_1(r_1 \varsigma_1) - z_2 \varsigma_2 \sigma_1(r_1 \varsigma_2)} \right] \tag{C3}$$

with

$$\chi_1(\varsigma_1 r_1) = \frac{K_1(\varsigma_1 r_1) I_0(\varsigma_1 r_1) + I_1(\varsigma_1 r_1) I_0(\varsigma_1 r_1)}{K_0(\varsigma_1 r_w) I_0(\varsigma_1 r_1) - I_0(\varsigma_1 r_w) K_0(\varsigma_1 r_1)}, \tag{C4}$$

$$\mu_1(\varsigma_1 r_1) = \frac{K_1(\varsigma_1 r_1) I_0(\varsigma_1 r_w) + I_1(\varsigma_1 r_1) I_0(\varsigma_1 r_w)}{K_0(\varsigma_1 r_1) I_0(\varsigma_1 r_w) - I_0(\varsigma_1 r_1) K_0(\varsigma_1 r_w)}, \tag{C5}$$

$$\sigma_1(\varsigma_2 r_1) = \frac{K_1(\varsigma_2 r_1)}{K_0(\varsigma_2 r_1)}, \tag{C6}$$

$$\tau_1(\varsigma_1 r_1) = \frac{K_1\left(\sqrt{\varsigma_1^2 + \alpha_1^2} r_1\right) I_0\left(\sqrt{\varsigma_1^2 + \alpha_1^2} r_w\right) + I_1\left(\sqrt{\varsigma_1^2 + \alpha_1^2} r_1\right) I_0\left(\sqrt{\varsigma_1^2 + \alpha_1^2} r_w\right)}{K_0\left(\sqrt{\varsigma_1^2 + \alpha_1^2} r_1\right) I_0\left(\sqrt{\varsigma_1^2 + \alpha_1^2} r_w\right) - I_0\left(\sqrt{\varsigma_1^2 + \alpha_1^2} r_1\right) K_0\left(\sqrt{\varsigma_1^2 + \alpha_1^2} r_w\right)}, \tag{C7}$$

$$\omega_1(\varsigma_2 r_1) = \frac{K_1\left(\sqrt{\varsigma_2^2 + \alpha_1^2} r_1\right)}{K_0\left(\sqrt{\varsigma_2^2 + \alpha_1^2} r_1\right)}. \tag{C8}$$

Note that the integrations for the first and third terms of Eq. (C2) with respect to z equal zero.

The result of inverse Laplace transform for Eq. (C3) using the Bromwich integral method [4] can be expressed as

$$Q_w(t) = \frac{1}{2\pi i} \int_{r_0 - i\infty}^{r_0 + i\infty} Q_w(p) e^{pt} dp, \tag{C9}$$

where i is an imaginary unit and r_0 is a larger constant than the real part of each singularity in complex plane. Eq. (C3) is a multiple value function and thus has a branch point at $p = 0$ and a branch cut extending from $p = 0$ to $p = -\infty$. The result of Eq. (C9) can be obtained by integration along the modified pathway of Bromwich integral, which consists of a close contour with a semicircle, circle, straight line parallel to the imaginary axis and two straight lines parallel to the branch cut.

The value of integration for the semicircle equals zero if its radius approaches infinity while the result of integration along the circle also equals zero if its radius approaches zero. Additionally, no pole exists in this complex plane. The variable p is expressed in terms of polar coordinate for describing a discontinuity at the branch cut. For the integration above the branch cut, let $p = r' e^{i\pi}$ and thus $\varsigma_i = i\sqrt{(S_{si}/K_{ri})r'}$ where r' represents the radius from the origin. In contrast, let $p = r' e^{-i\pi}$ and thus $\varsigma_i = -i\sqrt{(S_{si}/K_{ri})r'}$ for the integration below the branch cut. The result of integration for Eq. (C9) is therefore the sum of these two integrations expressed as

$$Q_w(t) = -\frac{1}{2\pi i} \int_0^\infty Q_w(r' e^{i\pi}) e^{-r't} dr' + \frac{1}{2\pi i} \times \int_0^\infty Q_w(r' e^{-i\pi}) e^{-r't} dr'. \tag{C10}$$

The Bessel functions can be expressed as a typical complex number of the sum of real and imaginary number as [17]

$$K_\nu\left(z e^{\pm \frac{1}{2}\pi i}\right) = \pm \frac{1}{2} \pi i e^{\mp \frac{1}{2}\nu\pi i} [-J_\nu(z) + i Y_\nu(z)], \tag{C11}$$

$$I_\nu\left(z e^{\pm \frac{1}{2}\pi i}\right) = e^{\pm \frac{1}{2}\nu\pi i} J_\nu(z), \tag{C12}$$

where ν represents the order of Bessel function. Substituting Eqs. (C11) and (C12) into the first term of Eq. (C10) and letting $u = \sqrt{S_{s1} r'/K_{r1}}$ yields

$$-\frac{1}{2\pi i} \int_0^\infty Q_w(r' e^{i\pi}) e^{-r't} dr' = 2\kappa_{r1} r_w z_1 h_w \int_0^\infty \times \frac{\Omega + i\Pi}{\Phi - i\Lambda} e^{-\frac{\kappa_{r1} u^2}{S_s} t} du, \tag{C13}$$

where u is a dummy variable for the integration. Similarly, the second term of Eq. (C10) can be expressed below based on $u = \sqrt{S_{s1} r'/K_{r1}}$ and Eqs. (C11) and (C12).

$$\frac{1}{2\pi i} \int_0^\infty Q_w(r' e^{-i\pi}) e^{-r't} dr' = 2\kappa_{r1} r_w z_1 h_w \int_0^\infty \times \frac{\Omega - i\Pi}{\Phi + i\Lambda} e^{-\frac{\kappa_{r1} u^2}{S_s} t} du. \tag{C14}$$

The sum of Eqs. (C13) and (C14) results in Eq. (20) which represents the injection rate at the wellbore. Note that the imaginary unit can be eliminated by the derivation of common denominator as $\Phi^2 + \Lambda^2$.

References

[1] Ramsay JG, Huber MI. The techniques of modern structural geology. Folds and fractures, vol. 2. London: Academic press; 1987.

[2] Matter JM, Takahashi T, Goldberg D. Experimental evaluation of in situ CO_2–water–rock reactions during CO_2 injection in basaltic rocks: implications for geological CO_2 sequestration. Geochem Geophys Geosyst 2007;8(2). doi:10.1029/2006GC001427.

[3] Kharaka YK, Cole DR, Hovorka SD, Gunter WD, Knauss KG, Freifeld BM. Gas-water-rock interactions in Frio formation following CO_2 injection: implications for the storage of greenhouse gases in sedimentary basins. Geology 2006;34(7):577–80.

[4] Metz B, Davidson O, Coninck HD, Loos M, Meyer L, editors. IPCC special report on carbon dioxide capture and storage. New York: Cambridge Univ Press; 2005.

[5] Nordbotten JM, Celia MA, Bachu S. Analytical solutions for leakage rates through abandoned wells. Water Resour Res 2004;40:W04204. doi:10.1029/2003WR002997.

[6] Kirkham D. Exact theory of flow into a partially penetrating well. J Geophys Res 1959;64(9):1317–27.

[7] Javandel I, Zaghim N. Analysis of flow to an extended fully penetrating well. Water Resour Res 1975;11(1):159–64.

[8] Al-Mohannadi N, Ozkan E, Kazemi H. Pressure-transient responses of horizontal and curved wells in anticlines and domes. SPEREE 2007:66–76.

[9] Yeh HD, Kuo CC. An analytical solution for heterogeneous and anisotropic anticline reservoirs under well injection. Adv Water Resour 2010;33:419–29. doi:10.1016/j.advwatres.2010.01.007.

[10] Stehfest H. Numerical inversion of Laplace transforms. Commun ACM 1970;13(1):47–9.

[11] Hildebrand FB. Advanced calculus for applications. 2nd ed. Englewood Cliffs, Nork York: Prentice-Hall; 1976.

[12] Chang YC, Yeh HD. A new analytical solution solved by triple series equations method for constant-head tests in confined aquifers. Adv Water Resour 2010;33:640–51. doi:10.1016/j.advwatres.2010.03.010.

[13] Yang SY, Yeh HD. Solution for flow rates across the wellbore in a two-zone confined aquifer. J Hyd Eng ASCE 2002;128(2):175–83. doi:10.1061/(ASCE)0733-9429(2002)128:2(175).

[14] Liou TS, Yeh HD. Conditional expectation for evaluation of risk groundwater flow and solute transport: one-dimensional analysis. J Hydrol 1997;199:378–402.

[15] Li X. Vertical resolution: gravity versus vertical gravity gradient. The Leading Edge; 2001.

[16] Andrews LA, Shivamoggi BK. Integral transforms for engineers and applied mathematicians. New York: Macmillen; 1988.

[17] Carslaw HS, Jaeger JC. Conduction of heat in solids. 2nd ed. London: Oxford University Press; 1959.